

Synthesis and Electrochemical Properties of CuFeO_2 as Negative Electrodes for Sodium-Ion Batteries

Yuhki Yui*, Yoko Ono, Masahiko Hayashi, Jiro Nakamura

Energy and Environment Systems Laboratories, NTT Corporation, Kanagawa 243-0198, Japan

Email address:

yui.yuhki@lab.ntt.co.jp (Y. Yui)

To cite this article:

Yuhki Yui, Yoko Ono, Masahiko Hayashi, Jiro Nakamura. Synthesis and Electrochemical Properties of CuFeO_2 as Negative Electrodes for Sodium-Ion Batteries. *American Journal of Physical Chemistry*. Vol. 4, No. 2, 2015, pp. 16-20. doi: 10.11648/j.ajpc.20150402.11

Abstract: This paper investigates the electrochemical properties of CuFeO_2 prepared by using a malate precursor method as negative electrodes for sodium-ion batteries. In the voltage range of 0.01 to 3.0 V, the oxide calcined at 750°C shows a poor cycle property of 27 mAh/g at 10 cycles, although it exhibits the large first discharge capacity of 579 mAh/g. The cycle property is improved to up to 122 mAh/g at 10 cycles by employing a cycle condition with the voltage range of 0.01 to 1.5 V. The results suggest that the sodium-ion insertion/extraction mechanism in CuFeO_2 would involve valence changes of Fe ions in the oxide from the Fe^{3+} state to Fe^0 state in the discharge process and from Fe^0 to Fe^{3+} in the charge process.

Keywords: Sodium-Ion Battery, Negative Electrode, CuFeO_2

1. Introduction

Lithium-ion batteries (LIBs) are widely used in mobile phones and notebook computers owing to their high voltages and high energy density. Furthermore, the market demand for large-sized LIBs as the power supply for electric vehicle has been increasing in recent years. However, lithium is expensive because it is not an abundant metal. On the other hand, sodium is abundant and cheap [1], and interest in sodium-ion batteries (SIBs) has been growing. Therefore, materials that have been studied for use as negative electrodes for SIBs include hard carbon [2 - 5], tin [6 - 8] and tin-based materials [9 - 10]. Hard carbon can be cycled more than 100 times, but its capacity is only about 250 mAh/g [2]. On the other hand, the capacities of tin and tin-based materials are about 500 mAh/g [7], but their cycle performance is poor. In addition, some oxide materials, such as $\text{Na}_2\text{Ti}_3\text{O}_7$ [11 - 12], $\text{Na}_4\text{Ti}_5\text{O}_{12}$ [13], TiO_2 [14 - 15], MoO_3 [16], Fe_3O_4 and $\alpha\text{-Fe}_2\text{O}_3$ [17], have been studied for use as SIBs' negative electrodes. However, most of these materials show small capacity or poor cycle performance, which leads to insufficient battery performance. In addition, most of the oxide materials show high voltage, which is why their energy density are low.

CuFeO_2 has a delafossite structure consisting of closely packed oxygen double layers, in which the octahedral sites are occupied by Fe^{3+} cations, and these double layers are

linked by monovalent Cu^+ ions with two-fold oxygen linear coordination [18]. CuFeO_2 has been studied as a negative electrode material for LIBs [19 - 20], and it exhibited a 475 mAh/g beyond 100 cycles. As reported in ref. [19], the reversible capacity of Li/CuFeO_2 cell is expected to correspond to 4 mol of Li per mole of CuFeO_2 , and the theoretical capacity is 694 mAh/g.

In this study, we investigated the electrochemical properties of CuFeO_2 as negative electrodes for SIBs. We performed X-ray diffraction (XRD) measurements and X-ray photoelectron spectroscopy (XPS) measurements of electrodes containing CuFeO_2 during cycling to examine the reaction mechanism involved in the crystallographic-structure changes in the oxide.

2. Experimental

CuFeO_2 was prepared by using a malate precursor method [19]. The precursor powder was obtained by evaporating a mixed aqueous solution of $\text{Cu}(\text{NO}_3)_2 \cdot 3\text{H}_2\text{O}$ (Kanto Chemical Co.), $\text{Fe}(\text{NO}_3)_3 \cdot 9\text{H}_2\text{O}$ (Kanto Chemical Co.), and malic acid (Kanto Chemical Co.). Then the precursor powder was calcined at 750 or 900°C for 10 h in Ar. The phases of the resulting powder were identified with a powder X-ray diffractometer (XRD, Rigaku, X-ray diffractometer RINT2000) using $\text{CuK}\alpha$ radiation. The morphology of the powder was observed by a scanning electron microscope

(SEM, JEOL Ltd., JSM-890) with accelerating voltage of 7 kV.

Working electrodes for electrochemical measurements were prepared by mixing CuFeO_2 powder, acetylene black as a conductive material, polyvinylidene difluoride (PVdF) binder in N-methylpyrrolidone, coating the mixture slurry on an Al sheet as a current collector, and finally drying it at 90°C in an oven. The electrochemical performance was evaluated with a 2032 coin-type cell using a working electrode (0.02 mm thick and 14 mm in diameter), a non-aqueous electrolyte (1 mol/l NaPF_6 / EC:DEC 1:1 in volume, Tomiyama Pure Chemicals Industries Ltd.), a polypropylene separator (Celgard, 19 mm in diameter), and sodium metal sheets (0.6 mm thick and 15 mm in diameter, Kanto Chemical Co.) as a counter electrode. All cells were assembled in an Ar-filled glove box (dew point $< -75^\circ\text{C}$). Cycling tests were performed with an automatic galvanostatic discharge-charge system unit (Hokuto Denko Corp. HJ1001SD8) at a current density of 25 mA/g between 0.01 and 3.0 V (or 1.5 V) at 25°C . Then, the cells were opened after the charge/discharge process in the Ar-filled glove box, and the working electrodes were soaked in dimethyl carbonate (Tomiyama Pure Chemicals Industries Ltd.) and dried in the glove box overnight. XRD measurements of the electrodes with discharged or charged states were performed. Inductively coupled plasma spectroscopy (ICP, Hitachi High-Technologies Co., SPS1700) was used to evaluate the composition of the $\text{Na}_x\text{-CuFeO}_2$ in the electrodes before and after charge/discharge processes. The sample solution for the ICP-AES analysis was prepared as follows. Working electrodes were removed from discharged/charged coin cells and washed with dimethyl carbonate (DMC) in the glove box. Then electrode materials were dissolved in a dilute acid mixture consisting of nitrohydrochloric acid, perchloric acid, sulfuric acid, and nitrohydrochloric acid. An X-ray photoelectron spectrometer (XPS) analysis was performed with a PHI XPS-5700 system using AlK_α radiation (1486.6 eV) to examine the binding energy for Fe2p of as-prepared, discharged, or charged electrodes. The binding energies for Fe2p were identified using the NIST database [21]

3. Results and Discussion

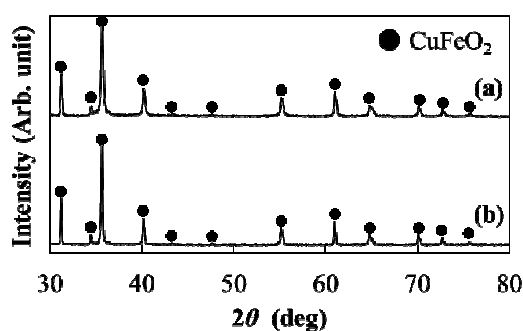


Figure 1. XRD patterns of obtained CuFeO_2 powder: (a) 750°C and (b) 900°C .

Figure 1 shows the powder XRD patterns of the sample

obtained at 750 or 900°C for 10 h in Ar. The XRD patterns well agree with that of hexagonal CuFeO_2 (PDF No. 00-039-0246). Furthermore, they are consistent with the pattern reported in the literature [19]. These results indicate that CuFeO_2 was obtained as a single phase. Figure 2 shows SEM images of the CuFeO_2 particles sintered at 750°C and 900°C . The oxide sintered at 750°C has the primary particle size of $0.3\text{--}0.5\ \mu\text{m}$. On the other hand, the oxide sintered at 900°C consist of primary particles of more than $1.0\ \mu\text{m}$, and the particles are aggregate by sintering at higher temperature.

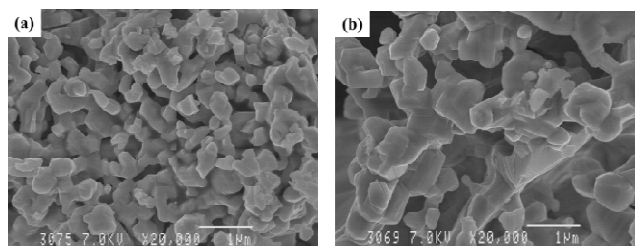


Figure 2. SEM images of obtained powder: (a) 750°C and (b) 900°C .

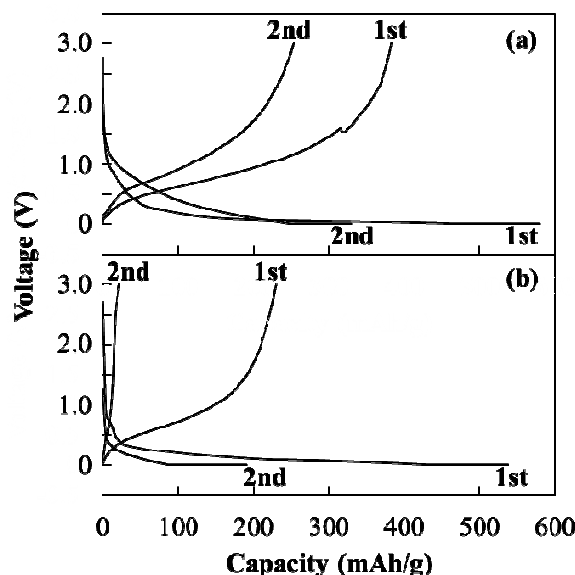


Figure 3. Discharge-charge curves of CuFeO_2 electrodes: (a) 750°C and (b) 900°C in the 0.01 to 3.0 V range at current density of 25 mA/hg.

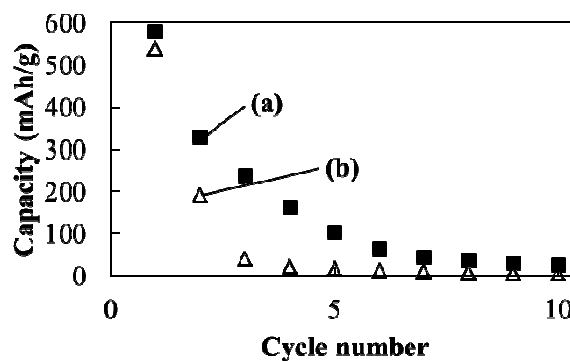


Figure 4. Cycle properties of CuFeO_2 electrodes: (a) 750°C and (b) 900°C in the 0.01 to 3.0 V range at current density of 25 mA/hg.

Figures 3 and 4 respectively show the first and second

discharge (Na-ion insertion)-charge (Na-ion extraction) curves and the cycle properties of a Na/CuFeO₂ (750, 900°C) in the voltage range of 0.01 to 3.0 V. In the first discharge profile of CuFeO₂ obtained at 750°C, the voltage drops rapidly to about 1.0 V from the open-circuit voltage of about 2.8 V and then decreases gradually to 0.01 V. In Li/CuFeO₂, the discharge plateau voltage was observed at around 1.0 V, and the first discharge and charge capacities were about 935 and 700 mAh/g [19]. This suggests that the reaction mechanism is different between Na/CuFeO₂ and Li/CuFeO₂. Na/CuFeO₂ could have higher energy density than Li/CuFeO₂, because it showed low voltage. The first discharge and charge capacities of CuFeO₂ obtained at 750°C were 579 (equivalent to 3.7 Na per CuFeO₂ mol) and 383 mAh/g (equivalent to 2.5 Na per CuFeO₂ mol), respectively. ICP analysis results revealed that 3.2 and 1.9 mol of sodium ions were inserted/extracted after the first discharge/charge processes (Table 1). These results are in good agreement with the values calculated from the discharge/charge capacities as shown in Fig. 3(a). The large irreversible capacity of about 200 mAh/g in the first cycle might be due to significant changes in the crystal structure with Na-ion insertion during the first discharge. The first discharge and charge capacities of the sample obtained at 900°C were 538 and 238 mAh/g, respectively. Since CuFeO₂ at 900°C has large particle size as shown in Fig. 2(b), Na ions might not easily insert into the CuFeO₂ bulk. That would explain why the capacity of the sample obtained at 900°C was smaller than that of the sample obtained at 750°C and why the over potential between discharge and charge voltage was higher than that of the one of the sample obtained at 750°C. Additionally, both oxides showed much higher second charge voltage than the first one. This led to a drastic decline to where the oxide at 750°C showed a very low discharge capacity retention of about 5% at the 10th cycle as shown in Fig. 4. This suggests that CuFeO₂ underwent severe crystallographic changes during the first cycle.

Figure 5 shows the XRD patterns of CuFeO₂ obtained at 750°C during the first cycle in the voltage range of 0.01 to 3.0 V. After the first discharge (Na-ion insertion), the peaks corresponding to CuFeO₂ almost completely disappeared as shown in Fig. 5(b). This result suggests that the CuFeO₂ crystalline phase might become amorphous phase. Moreover, new peaks assigned to NaCuO (PDF No. 01-071-2300) and Fe₃O₄ (PDF No. 00-003-0862) were observed. After the first charge, there were small peaks of CuFeO₂ and NaCuO peaks as shown in Fig. 5(c).

Table 1. Changes in sodium content, x , in Na _{x} -CuFeO₂ after the first dis-charge/charge process.

Process	x in Na _{x} -CuFeO ₂	
	From capacity	From ICP analysis
After first discharge	3.3	3.2
After first charge	2.2	1.9

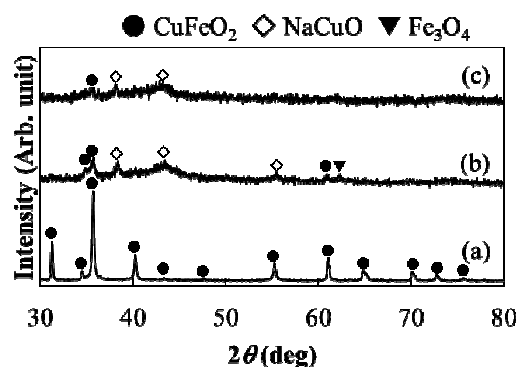


Figure 5. XRD patterns of (a) pristine CuFeO₂ electrodes, (b) after discharge, and (c) after charge.

XPS measurements provide information to examine the reaction mechanism, and the binding energies for Fe2p were identified using the NIST database. Figure 6 (a) shows the wide-scan spectrum of pristine CuFeO₂ electrodes. The Fe2p, Cu2p, O1s, F1s and C1s peaks are assigned as shown in Fig. 6(a). The typical narrow-scan spectra of Fe2p after discharge to 0.01 V and after charge to 3.0 V are shown in Fig. 6(b) for pristine electrodes. The Fe2p peak shifted toward lower binding energy from 711.2 (pristine, the Fe³⁺ state) to 710.5 eV (after discharge and after charge) as shown in Fig. 6(b).

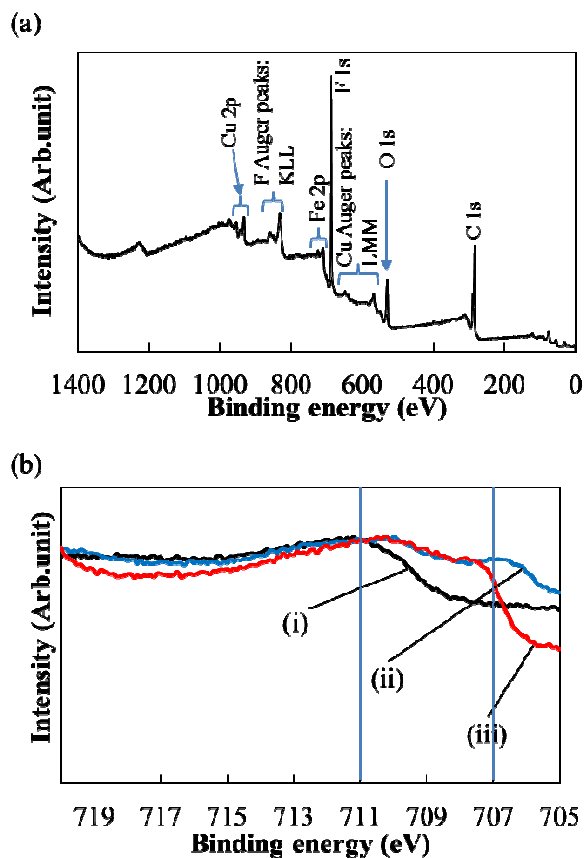


Figure 6. XPS spectra for CuFeO₂: (a) Wide scan and (b) Fe2p. (i) Pristine, (ii) after discharge, (iii) after charge.

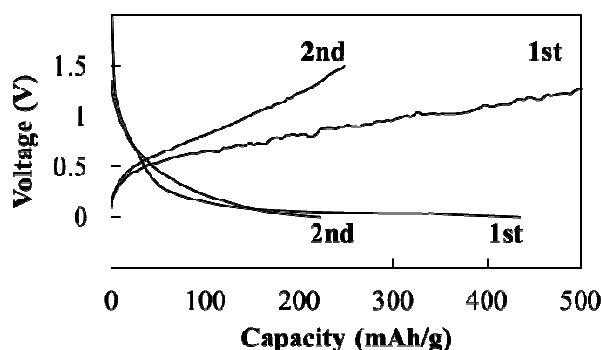


Figure 7. Discharge-charge curves of CuFeO_2 electrodes obtained at 750°C in the 0.01 to 1.5 V range at current density of 25 mAh/g.

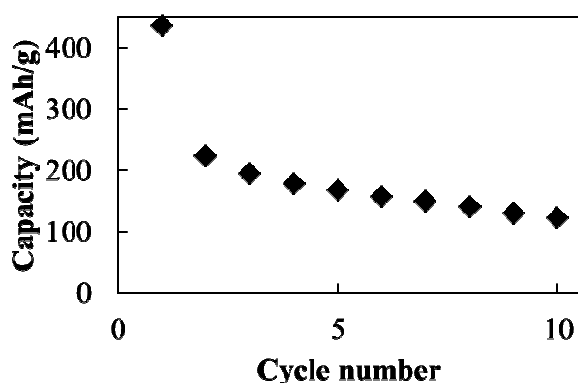


Figure 8. Cycle properties of CuFeO_2 electrodes obtained at 750°C in the 0.01 to 1.5 V range at current density of 25 mAh/g.

Additionally, a shoulder at 707.0 eV (the Fe^0 state) in the $\text{Fe}2p$ spectra appeared after discharge and disappeared after charge, indicating that the bonding state of the Fe atoms has changed. This change can be attributed to the change from the Fe^{3+} state to Fe^0 state due to discharging (Na-ion insertion). At the next charge, the Fe^0 state changes to the Fe^{3+} state by charging (Na-ion extraction). This indicates that the bonding state of the Cu atoms must have changed with the changing bonding state of the Fe atoms. In Na/CuFeO_2 , both of the bonding states and the crystal structure change during cycling. That is why Na/CuFeO_2 has a poor cycle performance.

In an attempt to improve the cycle performance, we carried out cycling tests under the discharge/charge condition with a narrower voltage range. Figures 7 and 8 show the first and second discharge-charge curves and the cycle properties of a Na/CuFeO_2 (750°C), respectively, in the voltage range of 0.01 to 1.5 V. The first and second discharge capacities were 435 and 223 mAh/g, respectively. These capacities in the voltage range of 0.01 to 1.5 V were smaller than those in the range of 0.01 to 3.0 V. The smaller capacity was due to the insufficient charge process as a result of the narrower voltage range. The larger discharge capacity of 122 mAh/g at the 10th cycle was obtained in the narrower voltage range, although the capacity at the 10th cycle was 27 mAh/g for the wide voltage condition. As described above, the cycle property was improved by employing a suitable discharge/charge voltage range.

4. Conclusions

CuFeO_2 powders were synthesized by using a malate precursor method. Their electrochemical properties as negative electrodes for SIBs were examined. The particle size of the oxide sintered at 750°C (0.3-0.5 μm) is smaller than the one sintered at 900°C (0.5-1.0 μm). The discharge capacity of the 750°C oxide (579 mAh/g) was larger than that of 900°C one (538 mAh/g) in the 0.01 to 3.0 V range. Na ions might easily insert into the bulk of the CuFeO_2 obtained at 750°C because of the small particles, which would explain its large capacity. The cycle properties were poor (750°C : 27 mAh/g up to 10 cycles). The reasons for the poor cycle performance are changes in the bonding states of the atoms and changes in the crystal structure during cycling. In the narrow voltage range of 0.01 to 1.5V, the cycle property was improved from 27 to 122 mAh/g at 10 cycle.

References

- [1] M. D. Slater, D. Kim, E. Lee, and C. S. Johnson, "Sodium-Ion Batteries," *Adv. Funct. Mater.*, 2013, 23, pp. 947-958.
- [2] S. Komaba, W. Murata, T. Ishikawa, N. Yabuuchi, T. Ozeki, T. Nakayama, A. Ogata, K. Gotoh, and K. Fujiwara, "Electrochemical Na Insertion and Solid Electrolyte Interphase for Hard-Carbon Electrodes and Application to Na-Ion Batteries" *Adv. Funct. Mater.*, 2011, 21, pp. 3859-3867.
- [3] X. Xia, M. N. Obrovac, and J. R. Dahn, "Comparison of the Reactivity of Na_xC_6 and Li_xC_6 with Non-Aqueous Solvents and Electrolytes," *Electrochem Solid State Lett.*, 2011, 14, pp.A130-133.
- [4] K. Gotoh, T. Ishikawa, S. Shimadzu, N. Yabuuchi, S. Komaba, K. Takeda, A. Goto, K. Deguchi, S. Ohki, K. Hashi, T. Shimizu, and H. Ishida, "NMR study for electrochemically inserted Na in hard carbon electrode of sodium ion battery," *J. Power Sources*, 2013, 225, pp.137-140.
- [5] D. A. Stevens, and J. R. Dahn, "High Capacity Anode Materials for Rechargeable Sodium-Ion Batteries," *J. Electrochem. Soc.*, 2000, 147, pp. 1271-1273.
- [6] L. D. Ellis, T. D. Hatchard, and M. N. Obrovac, "Reversible Insertion of Sodium in Tin," *J. Electrochem. Soc.*, 2012, 159, pp. A1801-1805.
- [7] S. Komaba, Y. Matsuura, T. Ishikawa, N. Yabuuchi, W. Murata, and S. Kuze, "Redox reaction of Sn-polyacrylate electrodes in aprotic Na cell," *Electrochem. Commun.*, 2012, 21, pp.65-68.
- [8] M. K. Datta, R. Epur, P. Saha, K. Kadakia, S. K. Park, and P. N. Kumta, "Tin and graphite based nanocomposites: Potential anode for sodium ion batteries," *J. Power Sources*, 2013, 225, pp.316-322.
- [9] Y. Yui, Y. Ono, M. Hayashi, Y. Nemoto, K. Hayashi, K. Asakura, and H. Kitabayashi, "Sodium-ion Insertion/Extraction Properties of Sn-Co Anodes and Na pre-doped Sn-Co Anodes," *J. Electrochem. Soc.*, 2015, 162, A3098-A3102.
- [10] A. M. Sukeshini, H. Kobayashi, M. Tabuchi, and H. Kageyama, "Physicochemical characterization of CuFeO_2 and lithium intercalation," *Solid State Ionics*, 2000, 128, pp.33-41.

- [11] H. Pan, X. Lu, X. Yu, Y.-S. Hu, H. Li, X.-Q. Yang, and L. Chen, "Sodium Storage and Transport Properties in Layered Na₂Ti₃O₇ for Room-Temperature Sodium-Ion Batteries," *Adv. Energy Mater.*, 2013, 9, pp.1186-1194.
- [12] P. Senguttuvan, G. Rousse, V. Seznec, J.-M. Tarascon, and M. R. Palacin, "Na₂Ti₃O₇: Lowest Voltage Ever Reported Oxide Insertion Electrode for Sodium Ion Batteries," *Chem. Mater.*, 2011, 23, pp.4109-4111.
- [13] P. J. Naeyaert, M. Avdeev, N. Sharma, H. B. Yahia, and C. D. Ling, "Synthetic, Structural, and Electrochemical Study of Monoclinic Na₄Ti₅O₁₂ as a Sodium-Ion Battery Anode Material," *Chem. Mater.*, 2014, 26, pp.7067-7072.
- [14] H. Xiong, M. D. Slater, M. Balasubramanian, C. S. Johnson, and T. Rajh, "Amorphous TiO₂ Nanotube Anode for Rechargeable Sodium Ion Batteries," *J. Phys. Chem. Lett.*, 2012, 2, pp.2560-2565.
- [15] L. Wu, D. Buchholz, D. Bresser, L. G. Chagas, and S. Passerini, "Anatase TiO₂ nanoparticles for high power sodium-ion anodes," *J. Power Sources*, 2014, 251, pp.379-385.
- [16] S. Hariharan, K. Saravanan, and P. Balaya, "α-MoO₃: A high performance anode material for sodium-ion batteries," *Electrochem. Commun.*, 2013, 31, pp.5-9.
- [17] S. Komaba, T. Mikumo, N. Yabuuchi, A. Ogata, H. Yoshida, and Y. Yamada, "Electrochemical Insertion of Li and Na Ions into Nanocrystalline Fe₃O₄ and α-Fe₂O₃ for Rechargeable Batteries," *J. Electrochem. Soc.*, 2010, 157, pp. A60-A65.
- [18] P. Dordor, J. P. Chaminade, A. Wichainchai, E. Marquestaut, J.P. Doumerc, M. Pouchard, and P. Hagenmuller, "Crystal growth and electrical properties of CuFeO₂ single crystals," *J. Solid State Chem.*, 1988, 75, pp.105-112.
- [19] L. Lu, J.-Z. Wang, X.-B. Zhu, X.-W. Gao, and H.-K. Liu, "High capacity and high rate capability of nanostructured CuFeO₂ anode materials for lithium-ion batteries," *J. Power Sources*, 2011, 196, pp.7025-7029.
- [20] A. M. Sureshini, H. Kobayashi, M. Tabuchi, and H. Kageyama, "Physicochemical characterization of CuFeO₂ and lithium intercalation," *Solid State Ionics*, 2000, 128, pp.33-41.
- [21] C. D. Wagner, C. J. Powell, J. W. Allison, and J. R. Rumble, "NIST X-ray Photoelectron Spectroscopy Database Version 2.0," National Institute of Standards and Technology, 1997.